Available online at www.sciencedirect.com
SCIENCE DIRECT®
ELSEVIER
Photonics and Nanostructures – Fundamentals and Applications 2 (2004) 103–110
PHOTONICS AND NANOSTRUCTURES
Fundamentals and Applications
www.elsevier.com/locate/photonics

Gap maps, diffraction losses, and exciton–polaritons in photonic crystal slabs

Lucio Claudio Andreani*, Dario Gerace, Mario Agio

INFM and Dipartimento di Fisica "A. Volta," Università di Pavia, via Bassi 6, 27100 Pavia, Italy

Received 15 June 2004; received in revised form 8 July 2004; accepted 8 July 2004
Available online 3 August 2004

Abstract

A theory of photonic crystal (PhC) slabs is described, which relies on an expansion in the basis of guided modes of an effective homogeneous waveguide and on treating the coupling to radiative modes and the resulting losses by perturbation theory. The following applications are discussed for the case of a high-index membrane: gap maps for photonic lattices in a waveguide; exciton–polariton states, when the PhC slab contains a quantum well with an excitonic resonance; propagation losses of line-defect modes in W1 waveguides, also in the presence of disorder; the quality factors of photonic nanocavities. In particular, we predict that disorder-induced losses below 0.2 dB/mm can be achieved in state-of-the-art samples by increasing the channel width of W1 waveguides.

PACS: 42.70.Qs; 42.82.Et; 71.36.+c; 78.20.Bh

Keywords: Photonic crystal slabs; Polaritons; Diffraction losses; Disorder; Photonic cavities

1. Introduction

Photonic crystals embedded in planar waveguides, also known as photonic crystal (PhC) slabs, can lead to a full control of light propagation because of the two-dimensional (2D) photonic lattice in the slab plane combined with dielectric confinement in the vertical direction [1,2]. Electromagnetic eigenmodes in PhC slabs can be either truly guided (if their frequency lies below the light line of the cladding material) or quasi-guided (if the frequency lies above the light line). Quasi-guided modes are subject to intrinsic radiative losses because of diffraction out of the slab plane. Truly guided modes are only subject to extrinsic losses due to disorder. Diffraction losses represent a crucial problem for prospective applications of PhC slabs to integrated photonic devices.

In this work, we present a theory of photonic modes and of radiation-matter interaction in PhC slabs that relies on an expansion of the magnetic field on the basis of guided modes of an effective homogeneous waveguide. Coupling to radiative modes of the effec-

* Corresponding author. Tel.: +39 0382 507491; fax: +39 0382 507563.
E-mail address: andreani@fisicavolta.unipv.it (L.C. Andreani).

1569-4410/$ – see front matter © 2004 Elsevier B.V. All rights reserved.
doi:10.1016/j.photonics.2004.07.003

tive waveguide is taken into account by perturbation theory and leads to a determination of diffraction losses. The theory allows calculation of the following quantities: photonic band dispersion and gap maps for 1D and 2D lattices embedded in a waveguide; the intrinsic losses of quasi-guided modes, due to the non-separable form of the dielectric modulation; the extrinsic losses of truly guided modes, by means of a Gaussian model of disorder; exciton–polariton states, when the PhC slab contains a quantum well with an excitonic resonance. Throughout this paper we consider the self-standing membrane (air bridge) as a prototype of a PhC slab with a strong refractive index contrast. In particular, we calculate propagation losses of line defect modes in W1 waveguides in the presence of structural disorder (modelled as random variations of hole radii in the triangular lattice) and Q-factors of photonic nanocavities.

2. Method

In order to formulate the method, we start from the second-order equation for the magnetic field,

$$\nabla \times \left[\frac{1}{\varepsilon(\mathbf{r})}\nabla \times \mathbf{H}\right] = \frac{\omega^2}{c^2}\mathbf{H}, \tag{1}$$

where $\varepsilon(\mathbf{r})$ is the spatially-dependent dielectric constant. If the magnetic field is expanded in an orthonormal set of basis states as $\mathbf{H}(\mathbf{r}) = \sum_\mu c_\mu \mathbf{H}_\mu(\mathbf{r})$, then Eq. (1) is transformed into a linear eigenvalue problem,

$$\sum_\nu \hat{H}_{\mu\nu} c_\nu = \frac{\omega^2}{c^2} c_\mu, \tag{2}$$

where the matrix $\hat{H}_{\mu\nu}$ (which is the analog of a quantum Hamiltonian for an electronic problem) is given by

$$\hat{H}_{\mu\nu} = \int \frac{1}{\varepsilon(\mathbf{r})}(\nabla \times \mathbf{H}^*_\mu(\mathbf{r}))\cdot(\nabla \times \mathbf{H}_\nu(\mathbf{r}))\,\mathrm{d}\mathbf{r}. \tag{3}$$

For the case of a PhC slab we have a waveguide along z and a periodic patterning in the xy plane. The basis set $\mathbf{H}_\mu(\mathbf{r})$ is chosen to consist of the guided modes of an effective waveguide, where each layer j has a homogeneous dielectric constant given by the spatial average of $\varepsilon_j(x,y)$. The index μ can be written as $\mu = (\mathbf{k}+\mathbf{G},\alpha)$, where $\mathbf{k}$ is the 2D Bloch vector, $\mathbf{G}$ is a reciprocal lattice vector and α labels the guided modes at wave vector $\mathbf{k}+\mathbf{G}$. The matrix elements (3) can be expressed in terms of the inverse dielectric tensor in each layer $\varepsilon_j^{-1}(\mathbf{G},\mathbf{G}')$, evaluated by a numerical inversion of the matrix $\varepsilon_j(\mathbf{G},\mathbf{G}')$ as in usual plane wave calculations.

The basis set consisting of the guided modes of the effective waveguide is orthonormal, but not complete, since the leaky modes of the waveguide are not included. Coupling to leaky modes produces a second-order shift of the mode frequency: neglect of this effect is the main approximation of the method. A comparison with exact scattering matrix calculations indicates that the second-order shift is quite small [3], at least for the low air fractions that are usually employed. When the guided modes are folded in the first Brillouin zone, many of them fall above the light line and become quasi-guided. Indeed, first-order coupling to leaky modes at the same frequency leads to a radiative decay, i.e., to an imaginary part of the frequency. This can be calculated by time-dependent perturbation theory, like in Fermi Golden Rule for quantum mechanics, and is given by

$$-\mathrm{Im}\left(\frac{\omega_k^2}{c^2}\right) = \pi\left|\hat{H}_{\mathrm{leaky,guided}}\right|^2 \rho\left(\mathbf{k};\frac{\omega_k^2}{c^2}\right), \tag{4}$$

where $\rho(\mathbf{k};\omega_k^2/c^2)$ is the 1D photonic density-of-states at fixed in-plane wave vector [4,5].

The effect of disorder is modelled by considering a random variation of hole radii within a large supercell, with a Gaussian probability function,

$$P(r) \propto \exp\left(\frac{-(r-\bar{r})^2}{2(\Delta r)^2}\right), \tag{5}$$

where the root mean-square deviation Δr of the radius is taken as a disorder parameter. The variations of hole size from the ideal value change the dielectric function to $\varepsilon_{\mathrm{dis}}(\mathbf{r})$ and give rise to a dielectric perturbation, $\Delta\varepsilon^{-1}(\mathbf{r}) = \varepsilon_{\mathrm{dis}}^{-1}(\mathbf{r}) - \varepsilon^{-1}(\mathbf{r})$, which couples both quasi- and truly guided modes into the radiative region and is also treated by perturbation theory.

3. Photonic bands and gap maps

A notable feature of the present method is that it leads to a determination of the photonic mode dispersion both below and above the light line. This allows

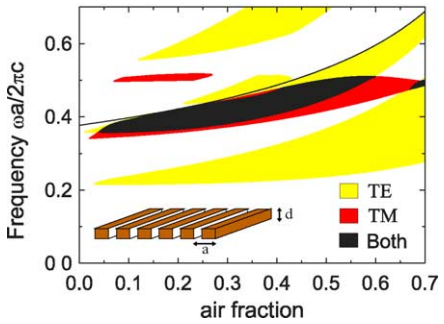

Fig. 1. Gap map of a 1D lattice of air stripes in a dielectric slab with $\varepsilon = 12$ and thickness $d/a = 0.4$. The solid curve is the cut-off of the second-order waveguide mode.

calculation of gap maps for photonic lattices embedded in a waveguide. As an example, in Fig. 1 we show the gap map of a 1D lattice of air stripes in a dielectric slab with $\varepsilon = 12$ and core thickness $d/a = 0.4$. Transverse electric (TE) and transverse magnetic (TM) polarizations are defined with respect to a vertical plane perpendicular to the stripes. TE and TM polarization are degenerate in the ideal 1D system; this degeneracy is removed in the slab, because of the effect of vertical confinement which is much more pronounced for TM than for TE polarization. As a result, a complete band gap for all polarizations does not generally occur. For the parameters of Fig. 1, a complete photonic gap is formed between the second-order TE gap and the first-order TM gap. A systematic study of gap maps of 2D and 1D photonic lattices in a waveguide is presented in Refs. [3,6], respectively.

An example of complex frequency dispersion of quasi-guided modes is given in Fig. 2, which shows the real and imaginary parts of frequency as a function of wave vector and compares them to the reflectance of a plane wave incident on the crystal surface calculated by the scattering-matrix method [7]. The positions of the spectral features in reflectance as a function of the incidence angle are seen to correspond to the dispersion of the real part of the frequency in Fig. 2a; the wave-vector component parallel to the surface is given by $k = (\omega/c)\sin\theta$. The linewidths of the resonances also change with the incidence angle and correspond to the imaginary part of the frequency shown in Fig. 2c. For example, the first even band has a linewidth that increases as a function of wave vector, until it drops to zero at the light cone; the third even band has a finite linewidth at $\mathbf{k} = 0$ (indeed it has dipolar symmetry at the Γ point) which decreases as a function of wave vector. These and other features can be recognized in the reflectance curves of Fig. 2b. Notice that the small values of $\mathrm{Im}(\omega)$ in Fig. 2c justify the use of perturbation theory. The behavior of $\mathrm{Im}(\omega)$ as a function of dielectric contrast and air fraction is discussed in Ref. [5].

4. Exciton–polaritons in photonic crystal slabs

Exciton–polaritons are the mixed modes of the electromagnetic field and an excitonic resonance, and are a well established concept in solid state

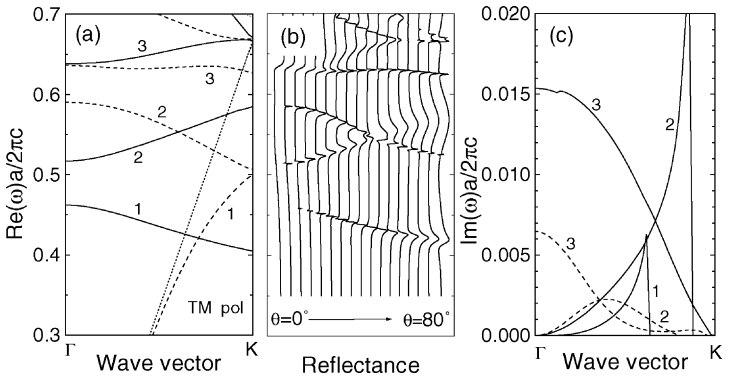

Fig. 2. (a) Photonic mode dispersion (real part of frequency), (b) reflectance spectra from 0 to 80° in steps of 5°, (c) imaginary part of frequency calculated for a membrane with $\varepsilon = 12$ and $d/a = 0.3$, patterned with a triangular lattice of holes with $r/a = 0.3$. All curves are calculated for TM-polarized modes along the ΓK orientation. Solid (dashed) lines refer to even (odd) modes with respect to a horizontal mirror plane. The dotted line in (a) is the light line in air.

physics [8]. Polaritonic effects in PhC slabs infiltrated with organic materials have been already shown experimentally[9] and studied theoretically[10,11] on a classical basis.

Here we describe a quantum theory of exciton polaritons in semiconductor-based PhC slabs. The method described in Section 2 allows calculation of the coefficients of the electromagnetic field through the solution of the linear system (2). By imposing the commutation relations on the classical fields in the Coulomb gauge, we obtain a description of the electromagnetic field in terms of creation/annihilation operators for its quanta, represented by the classical eigenmodes. The active material consists of one or more quantum wells (QWs) with an excitonic resonance, and we assume that the QW is placed in the slab with the same periodic pattern as the PhC. This leads to confinement of the exciton center-of-mass in the dielectric region. The second-quantized Hamiltonian, including the radiation-matter interaction, is written as

$$\hat{H} = \sum_{\mathbf{k},n} \hbar\omega_{\mathbf{k}n}\hat{a}^{\dagger}_{\mathbf{k}n}\hat{a}_{\mathbf{k}n} + \sum_{\mathbf{k},\nu} \hbar\Omega_{\mathbf{k}\nu}\hat{b}^{\dagger}_{\mathbf{k}\nu}\hat{b}_{\mathbf{k}\nu} + i\sum_{\mathbf{k},n,\nu} C_{\mathbf{k}n\nu}(\hat{a}_{\mathbf{k}n} + \hat{a}^{\dagger}_{-\mathbf{k}n})(\hat{b}^{\dagger}_{\mathbf{k}\nu} - \hat{b}_{-\mathbf{k}\nu}) + \sum_{\mathbf{k},\nu,n_1,n_2} \frac{C^{*}_{\mathbf{k}n_1\nu}C_{\mathbf{k}n_2\nu}}{\hbar\Omega_{\mathbf{k}\nu}}(\hat{a}_{-\mathbf{k}n_1} + \hat{a}^{\dagger}_{\mathbf{k}n_1})(\hat{a}_{\mathbf{k}n_2} + \hat{a}^{\dagger}_{-\mathbf{k}n_2}). \quad (6)$$

The first term describes free photon modes; $\hat{a}_{\mathbf{k}n}$ ($\hat{a}^{\dagger}_{\mathbf{k}n}$) is the destruction (creation) operator of a photon with band number n and complex frequency $\omega_{\mathbf{k}n}$. The excitonic problem is treated by solving Schrödinger's equation for the center-of-mass envelope function in a piecewise constant potential. The corresponding destruction (creation) operators are $\hat{b}_{\mathbf{k}\nu}$ ($\hat{b}^{\dagger}_{\mathbf{k}\nu}$) with eigenvalues $\hbar\Omega_{\mathbf{k}\nu}$. The coupling matrix elements are given by

$$C_{\mathbf{k}n\nu} = \left(\frac{e^2\hbar\Omega^2_{\mathbf{k}\nu}}{2\varepsilon_0\omega_{\mathbf{k}n}}\right)^{1/2} \left\langle \Psi^{(\mathrm{exc})}_{\mathbf{k}\nu} \middle| \sum_j \mathbf{E}_{\mathbf{k}n}(\mathbf{r}_j)\cdot\mathbf{r}_j \middle| 0 \right\rangle, \quad (7)$$

where $\Psi^{(\mathrm{exc})}_{\mathbf{k}\nu}$ is the exciton wavefunction, $\mathbf{E}_{\mathbf{k}n}$ is the electric field profile for the photonic mode, and the sum is over all QW electrons. Diagonalization of Hamiltonian (6) leads to the full spectrum of mixed photon-exciton modes. Polaritons are formed either when the exciton interacts with a truly guided photonic mode, or when it couples to a quasi-guided mode whose radiative linewidth is smaller than the exciton–photon coupling (7). The problem is also treated, for comparison, on a semiclassical basis by calculating the surface reflectance at varying angles of incidence with the scattering matrix method [7], including the excitonic resonance via a dispersive dielectric function in the QW layer. Result for 1D lattices of air stripes have been previously reported [12].

As an example, we consider here a self-standing membrane containing a QW layer at its center (see inset of Fig. 3b) patterned with a triangular lattice of holes. Fig. 3 shows the formation of PhC polaritons for TE-polarized modes along the ΓM direction. The excitonic resonance is placed at 1.58 eV and the exciton interacts with two quasi-guided photonic modes, see Fig. 3a. The intrinsic radiative width is about 1 meV at 1.58 eV, while the coupling energy is on the order of a few meV. This gives rise to coupled modes with two anti-crossings, as shown in Fig. 3b. The reflectance spectra in Fig. 3c display resonant features that correspond to the excitation of polariton modes above the light line and nicely reproduce the exciton–polariton dispersion curves. The results of quantum and semiclassical theories are in full agreement with each other. Notice that the polariton splitting at resonance is ~ 10 meV, which is larger than the typical values measured in III–V microcavities [13,14]. This is due to the strong field confinement in the slab waveguide, as compared to semiconductor

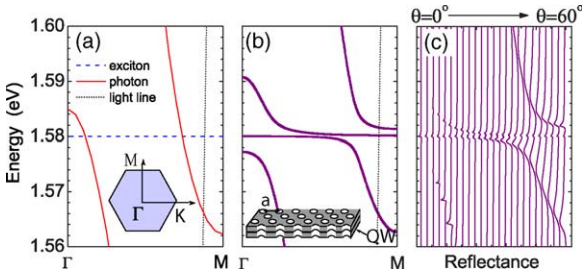

Fig. 3. (a) Dispersion of the uncoupled photon and exciton modes, (b) dispersion of exciton–polaritons obtained by the full quantum theory, and (c) reflectance spectra from 0 to 60° in steps of 2.5°. All curves refer to TE-polarized modes along the ΓM symmetry direction. Parameters: $\varepsilon = 12$, $a = 400$ nm, $d/a = 0.2$, $r/a = 0.3$, a single 8 nm wide QW with an oscillator strength per unit area $f/S = 8.4 \times 10^{12}$ cm^{-2}.

microcavities where the electromagnetic field has a sizeable penetration length in the distributed Bragg reflectors.

5. Propagation losses and effect of disorder in W1 waveguides

We consider a line defect consisting of a missing row of holes along the ΓK direction of the triangular lattice: this is called a W1 waveguide. The structure is shown in Fig. 4a (inset). The channel width w equals $w_0 \equiv \sqrt{3}a$, if the positions of the surroundings holes are those of the triangular lattice, but waveguides with reduced or increased channel widths have also been realized [15,16]. The W1 waveguide supports defect modes in the photonic gap, which opens only for states even with respect to a horizontal reflection plane. The lowest TE defect mode (spatially even with respect to the vertical midplane through the line defect) is mainly index-guided, i.e., it is confined laterally by the discontinuity of the refractive index between the waveguide and the surrounding patterned material. Its frequency-wave vector dispersion is shown in Fig. 4a.

We calculate the imaginary part of the frequency of the defect mode, the group velocity v_g and the propagation losses given by $2\mathrm{Im}(k) = 2\mathrm{Im}(\omega)/v_g$ (the loss in dB is given by $4.34 \times 2\mathrm{Im}(k)$). In Fig. 4b we show the imaginary part of the frequency of the defect mode as a function of the degree of disorder Δr.[1] Above the light line the intrinsic losses dominate and coincide with those previously calculated [17], except for a very large amount of disorder. Below the light line the losses are purely extrinsic and fall to much lower values. They grow quadratically with the disorder parameter, Δr, as expected for an elastic scattering mechanism in the perturbative limit.

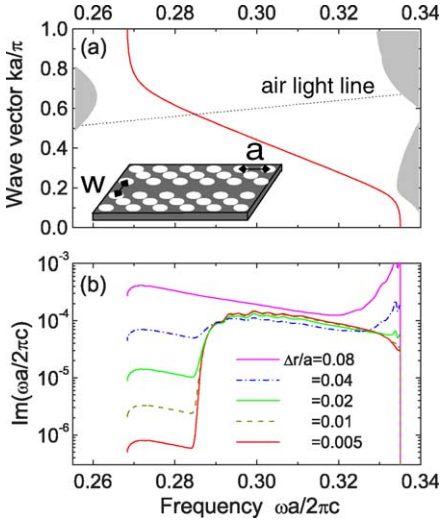

Fig. 4. (a) Dispersion of the defect mode, (b) imaginary part of frequency for different values of the disorder parameter $\Delta r/a$. Parameters of the air bridge structure are: $\varepsilon = 12$, $d/a = 0.5$, $r/a = 0.28$, W1 waveguide ($w = w_0 \equiv \sqrt{3}a$).

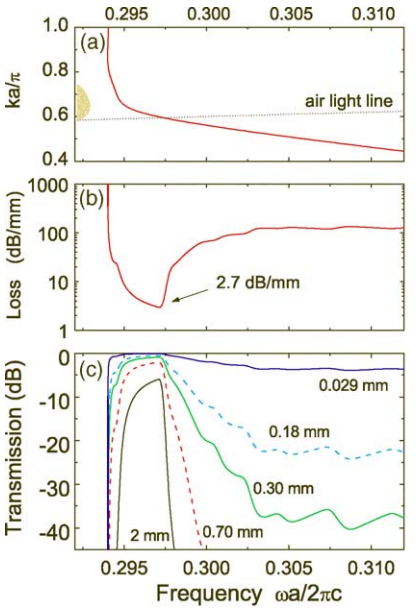

Fig. 5. (a) Dispersion of the defect mode, (b) propagation loss, (c) transmission spectra for different sample lengths with the parameters of the experiment of Ref. [18]: W1 waveguide in a Si slab with $\varepsilon = 12$, $d = 220$ nm, $a = 445$ nm, $r/a = 0.37$, $\Delta r = 5$ nm.

In Fig. 5 we show a comparison of the calculated propagation losses with a recent experiment performed on W1 waveguides in Si membranes [18], assuming the experimental structure and the quoted disorder parameter $\Delta r = 5$ nm. The defect mode is guided for frequencies below $\omega a/(2\pi c) = 0.297$ (Fig. 5a). The propagation loss in Fig. 5b has a minimum of 2.7 dB/mm when the defect mode crosses the light

[1] The calculations employ also a supercell in the direction perpendicular to the line defect with an average over different supercell widths, as explained in Ref. [17]. An additional average over different disorder distributions is taken in order to reproduce a statistical ensemble.

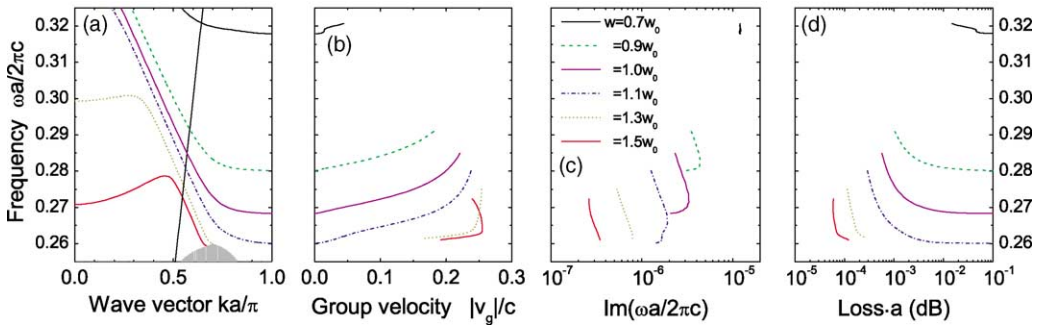

Fig. 6. (a) Dispersion of the defect mode, (b) group velocity, (c) imaginary part of frequency, (d) propagation loss for different values of the channel width w. Parameters of the air bridge structure are: $\varepsilon = 12$, $d/a = 0.5$, $r/a = 0.28$, $\Delta r/a = 0.01$. The results in (b), (c), and (d) are shown only for frequencies below the crossing with the light line (straight line in (a)).

line. This result is in amazingly good agreement with the experimental value 2.4 dB/mm. The losses increase rapidly both below the light line, due to the decreased group velocity of the defect mode, and above the light line because of the onset of intrinsic losses. The loss results can be shown in the form of transmission spectra for different PhC waveguide lengths, as in Fig. 5c. The comparison with the measured spectra (see Fig. 6 of Ref. [18]) is very satisfactory. It can be concluded that the present model gives an adequate account of disorder-induced losses measured in W1 waveguides, when state-of-the-art values for the roughness are assumed.

Results for disorder-induced losses as a function of core thickness and air fraction, as well as calculations in Silicon-On-Insulator (SOI) structures, are presented in Ref. [19]. Here, we shall discuss the dependence of the losses on the channel width for W1-type waveguides in an air-bridge structure. In Fig. 6 we show the defect mode dispersion, group velocity, imaginary part of frequency and propagation losses for waveguides with channel width w ranging from $0.7w_0$ to $1.5w_0$. The frequencies of the defect mode decrease with an increasing channel width. Moreover, the dispersion is modified in such a way that the group velocity at the crossing point with the light line increases and takes a maximum value close to $c/n \sim 0.25$ for waveguides with the largest values of w.[2] The results of Figs. 6c and d, which assume a disorder parameter $\Delta r = 0.01a$, can be scaled to other values of Δr by using the quadratic dependence discussed previously. The imaginary part of the frequency shown in Fig. 6c decreases rapidly for increasing channel width. This behavior, similar to the one occurring above the light line [17], follows from increasing localization of the electromagnetic field in the dielectric (channel) region, where it is less affected by fluctuations of the hole diameter. As a consequence of both the lower $\mathrm{Im}(\omega)$ and the higher v_g, the propagation loss shown in Fig. 6d is minimum for channel width $w = 1.5w_0$. By considering also the spatially odd defect mode, it can be shown that the waveguide with $w = 1.5w_0$ is truly monomode. The minimum loss $\sim 6 \times 10^{-5}$ in dimensionless units becomes about 0.15 dB/mm when divided by a lattice constant $a = 420$ nm (for a working wavelength $\lambda = 1.55\,\mu$m). Thus, we predict that propagation losses on the order of 0.15 dB/mm can be obtained in monomode waveguides with state-of-the-art values for the roughness ($\Delta r = 4$ nm), by increasing the channel width to $w = 1.5w_0$. We notice that such losses are comparable to those of silicon wires in the monomode region [20,21].

6. Photonic cavities

Point defects in PhC slabs behave as 0D cavities and support localized modes in the photonic gap. Cavity modes are always subject to intrinsic losses, as they have no wave vector and are coupled to the continuum of leaky slab modes by the dielectric

[2] Reduced-width waveguides with large group velocity have been demonstrated [15]: however, the mode considered in Ref. [15] is not the one shown in Fig. 6, but rather a lower one at frequencies lying close to the band edge.

modulation. Still, photonic cavities with large quality factor Q and small mode volumes can be defined. The quality factor can be increased by a momentum-space design, which allows reducing the radiative component of the confined photonic mode [22,23]. In real space, this corresponds to changing the position or size of the nearby holes. Up to now, the best performing cavity consists of three missing holes along the ΓK direction of the triangular lattice. By using the principle of "gentle confinement," which consists of shifting the positions of the holes close to the defect, Q-factors as high as 45,000 have been demonstrated [23].

Within the present method, the quality factor is calculated as $Q = \omega/(2\mathrm{Im}(\omega))$, by introducing a supercell in two directions and evaluating $\mathrm{Im}(\omega)$ in perturbation theory. We focus on cavities with one, two, or three missing holes in the triangular lattice (L1, L2, L3 defect) and consider a displacement or a shift of the nearby holes in the ΓK direction, as illustrated in Fig. 7. We calculate only intrinsic losses, i.e., we do not include the effect of disorder which is left for further analysis.

In Fig. 8 we show the quality factor as a function of (a) hole displacement and (b) hole shrinking. All curves have a pronounced maximum, confirming that the Q-factor is indeed increased by gentle confinement. For the case of the L3 defect with hole displacement, we find $Q = 45{,}000$ for $\Delta x/a = 0.15$, in agreement with the experimental results of Ref. [23]. The maximum calculated value is $Q \sim 1.5 \times 10^5$ at $\Delta x/a = 0.18$. The experimental values for $\Delta x/a = 0.2$ and 0.25 are lower than the theoretical ones.

Turning now to the case of hole shrinking, we notice that the maximum of the Q-factor as a function of $\Delta r/a$ is broader, implying that the structure may be more tolerant to small imperfections in fabrication. When the two nearby holes are shrunk to zero radius,

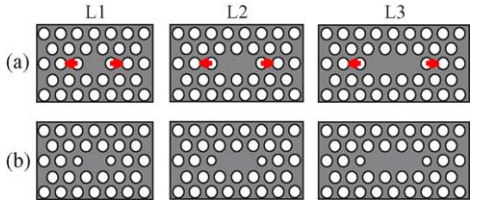

Fig. 7. Schematic structure of L1, L2, L3 point defects with (a) hole displacement and (b) hole shrinking.

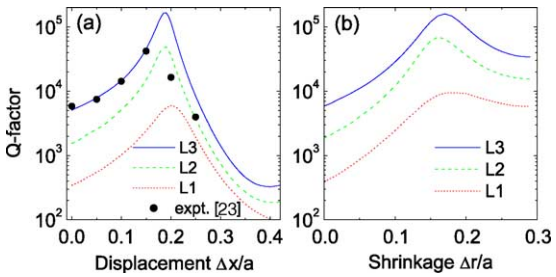

Fig. 8. Quality factor for L1, L2, L3 defects in a silicon membrane with $\varepsilon = 12$, $a = 420$ nm, $d/a = 0.6$, $r/a = 0.29$ as a function of (a) displacement and (b) shrinking of the two holes close to the defect along the ΓK direction (see Fig. 7).

that is $\Delta r/a = 0.29$, the curve relative to the Ln defect tends to the value for the L(n+2) defect at $\Delta r = 0$. The results of Fig. 8 show clearly that an L3 cavity with either hole displacement or hole shrinking has a higher Q than a bare L5 cavity.

7. Conclusions

The approach to PhC slabs consisting on an expansion in the basis of guided modes and on treating coupling to leaky modes by perturbation theory proves to be an efficient method for calculating photonic bands, gap maps, and diffraction losses for modes below and above the light cone. This approach is especially suited for PhC slabs with strong refractive index contrast. Line and point defects are treated by introducing a supercell, like in the usual plane-wave calculations. The formulation allows description of the effect of disorder on radiative losses by means of a model of random variations of hole size, or by related models currently under investigation. Also, the knowledge of electric and magnetic field profiles is the starting point for a quantum theory of exciton–polaritons in PhC slabs.

The main results discussed here are as follows. Gap maps of photonic lattices in a waveguide differ considerably from their 1D or 2D counterparts. Exciton–polaritons can form in PhC slabs made of III–V semiconductors with quantum wells, both below and above the light line: in the latter case the eigenmodes are radiative and can be probed by surface reflectance. Results for radiative losses in W1 waveguides and for Q-factor of photonic cavities have been

presented. In particular, disorder-induced losses grow quadratically with the disorder parameter and decrease while increasing the waveguide width. Assuming the same roughness parameter as in state-of-the-art samples ($\Delta r \sim 4$ nm), we predict that losses ~ 0.15 dB/mm can be achieved in high-index membranes using waveguides with increased channel width $w = 1.5w_0$.

Acknowledgments

This work was supported by MIUR through the Cofin program and by INFM through PRA PHOTONIC.

References

[1] K. Sakoda, Optical Properties of Photonic Crystals, Springer, Berlin, 2001.
[2] S.G. Johnson, J.D. Joannopoulos, Photonic Crystals: The Road from Theory to Practice, Kluwer, Dordrecht, 2002.
[3] L.C. Andreani, M. Agio, IEEE J. Quant. Electron. 38 (2002) 891.
[4] T. Ochiai, K. Sakoda, Phys. Rev. B 64 (2001) 045108.
[5] L.C. Andreani, Phys. Status Solidi (b) 234 (2002) 139.
[6] D. Gerace, L.C. Andreani, Phys. Rev. E 69 (2004) 056603.
[7] D.M. Whittaker, I.S. Culshaw, Phys. Rev. B 60 (1999) 2610.
[8] L.C. Andreani, Electron and Photon Confinement in Semiconductor Nanostructures, in: B. Deveaud, A. Quattropani, P. Schwendimann (Eds.), IOS Press, Amsterdam, 2003, p. 105.
[9] T. Fujita, Y. Sato, T. Kuitani, T. Ishihara, Phys. Rev. B 57 (1998) 12428.
[10] A.L. Yablonskii, E.A. Muljarov, N.A. Gippius, S.G. Tikhodeev, T. Fujita, T. Ishihara, J. Phys. Soc. Jpn. 70 (2001) 1137.
[11] R. Shimada, A.L. Yablonskii, S.G. Tikhodeev, T. Ishihara, IEEE J. Quant. Electron. 38 (2002) 872.
[12] D. Gerace, M. Agio, L.C. Andreani, Phys. Status Solidi (c) 1 (2004) 446.
[13] C. Weisbuch, M. Nishioka, A. Ishikawa, Y. Arakawa, Phys. Rev. Lett. 69 (1992) 3314.
[14] M.S. Skolnick, T.A. Fisher, D.M. Whittaker, Semicond. Sci. Technol. 13 (1998) 645.
[15] M. Notomi, K. Yamada, A. Shinya, J. Takahashi, C. Takahashi, I. Yokohama, Phys. Rev. Lett. 87 (2001) 253902.
[16] M. Notomi, A. Shinya, K. Yamada, J. Takahashi, C. Takahashi, I. Yokohama, IEEE J. Quant. Electron. 38 (2002) 736.
[17] L.C. Andreani, M. Agio, Appl. Phys. Lett. 82 (2003) 2011.
[18] S.J. McNab, N. Moll, Y.A. Vlasov, Opt. Express 11 (2003) 2927.
[19] D. Gerace, L.C. Andreani, Opt. Lett. 29 (2004), in press.
[20] K.K. Lee, D.R. Lim, H.-C. Luan, A. Agarwal, J. Foresi, L.C. Kimerling, Opt. Lett. 26 (2001) 1888.
[21] Y.A. Vlasov, S.J. McNab, Opt. Express 12 (2004) 1622.
[22] K. Srinivasan, O. Painter, Opt. Express 10 (2002) 670.
[23] T. Akahane, T. Asano, B.-S. Song, S. Noda, Nature 425 (2003) 944.